Korean J. Chem. Eng., 37(2), 341-349 (2020)
DOI: 10.1007/s11814-019-0451-3

pISSN: 0256-1115
eISSN: 1975-7220

Hydrate seeding effect on the metastability of CH_4 hydrate

Seungjun Baek, Wonhyeong Lee, Juwon Min, Yun-Ho Ahn, Dong Woo Kang, and Jae W. Lee†

Department of Chemical and Biomolecular Engineering, Korea Advanced Institute of Science and Technology (KAIST), 291 Daehak-ro, Daejeon 34141, Korea

(*Received 7 October 2019 • accepted 1 December 2019*)

Abstract−Cyclopentane (CP) hydrate seeds can lead to nucleation of CH_4 hydrate with a lower supersaturation; the concept of nucleation potential was applied to estimate the metastable zone width (MSZW) of CH_4 hydrate. To verify the crystal structure of CH_4 hydrate formed from the CP hydrate seeds, the hydrate samples were analyzed by high resolution powder diffraction (HRPD). 1 wt% of CP hydrates in the system reduced the MSZW of CH_4 hydrate from 3.39 K to 1.32 K, and showed synergetic performance with sodium dodecyl sulfate (SDS). From the hydrate nucleation theory, SDS is able to decrease the effective surface energy for heterogeneous nucleation on the stainless steel wall, but the CP hydrate seeds provide new nucleation sites with even lower surface energy than that of the stainless steel wall. Hence, the nucleation rate depends on the amount of CP hydrate seeds, and the kinetic parameter can be estimated from the concentration of nucleation sites on the CP hydrate seeds. Also, the MSZW of CH_4 hydrate was satisfactorily correlated with the amount of CP hydrate seeds by the cumulative nucleation potentials using estimated kinetic parameters.

Keywords: Methane Hydrates, Cyclopentane Hydrates, Hydrate Seed Crystals, Hydrate Nucleation, Metastable Zone Width

INTRODUCTION

Gas hydrates are ice-like crystalline inclusion compounds that are constructed from water molecules showing specific crystal cavities surrounded by three dimensional hydrogen-bonding networks. Small guest molecules occupy a vacancy of these cavities, and the occupation of guests stabilizes the hydrate structures by physical interactions with host water molecules. The configuration of guest molecules in hydrate cavities affects crystal lattices, and thus the geometry of guest molecules is a typical standard to determine the type of hydrate structure: structure I (sI, cubic $Pm\bar{3}n$, $2{\cdot}5^{12}+6{\cdot}5^{12}6^2$, 46 H_2O), structure II (sII, cubic $Fd\bar{3}m$, $16{\cdot}5^{12}+8{\cdot}5^{12}6^4$, 136 H_2O), and structure H (sH, hexagonal $P6/mmm$, $3{\cdot}5^{12}+2{\cdot}4^3 5^6+1{\cdot}5^{12}6^8$, 34 H_2O). Structural and inclusion properties of hydrate crystals have been verified by spectroscopic analyses and molecular simulations [1-5], and also their thermodynamic and kinetic properties are widely investigated with new hydrate-formers or chemical additives to seek practical applications in various fields [6-11].

To meet the increasing demand for natural gas, many studies have focused on developing natural gas storage to improve the industrial applicability [12]. At this point, artificially synthesized gas hydrates are also prominent natural gas storage materials due to mild storage conditions and water-based techniques. Furthermore, the hydrate medium has good storage capacity: 170 volumes of methane, which is the primary component of typical natural gas, can be stored in a unit volume of hydrate crystals at standard conditions. However, the utilization of hydrate as a storage medium has a critical limitation for slow nucleation and growth without mechanical agitation or chemical addition. Similar to other crystallization processes, the first hurdle in forming gas hydrate is the long induction time [12], and thus it is necessary to understand which kinetic factors are related with the hydrate nucleation process and how additives can affect this process.

Several studies have measured the induction time to verify the kinetics of hydrate nucleation and suggested theoretical models to predict the nucleation behaviors [13]. Kashchiev et al. reported an empirical correlation based on the general expression of the crystal nucleation rate with experimental sets of induction time [14]. From the formula for the rate of nucleation, they considered the difference between gas fugacity in the liquid and equilibrium fugacity as a driving force for the hydrate nucleation process and determined model parameters via linear regression between the logarithm of induction time and the supersaturation ratio. Also, an overall kinetic model of gas hydrate nucleation was derived with a single gas component in an aqueous solution for homogeneous and heterogeneous nucleation [15]. The derivation started from the difference of the chemical potentials between hydrate crystallite units in the solution and solid hydrate phases to define the driving force of hydrate nucleation. Considering the effective surface energy and kinetic parameters in terms of homogeneous and heterogeneous nucleation, the mathematical expressions for the rate and the induction time of hydrate nucleation were derived [14-16].

The concept of accumulation of nucleation potential (or probability) has been proposed to predict the hydrate nucleation behavior in non-isothermal systems. It is assumed that nucleation starts after achieving the density or potential of accumulated crystallites to a certain critical or detectable point, the same as the induction time in the isothermal process. Through this method, several studies estimated the metastable zone width (MSZW) [17,18], interfa-

†To whom correspondence should be addressed.
E-mail: jaewlee@kaist.ac.kr

cial energy, and the pre-exponential factor in the nucleation process [19]. Also, the effect of kinetic hydrate inhibitors on the hydrate formation was analyzed with the mathematical and empirical distribution [20-22].

In this study, we introduce the effect of cyclopentane (CP) hydrate seeds on the metastable zone width of CH_4 hydrate by analyzing the variation of measured MSZW with cumulative nucleation potentials for hydrate nucleation [14-17]. In our previous work, we verified the promotion effect of CP hydrate seeds on the overall kinetics of CH_4 hydrate formation in the isothermal system; however, the promotion mechanism was investigated with only morphological behavior during the hydrate crystallization [23]. Thus, we analyzed how the CP hydrate seeds induce rapid formation of different hydrate crystals with a theoretical approach on the crystal nucleation. First, we obtained the crystal structure of CH_4 hydrate using synchrotron high resolution powder diffraction (HRPD) and compared the HRPD patterns of binary (CP+CH_4 or tetrahydrofuran (THF)+CH_4) hydrates. Since CP generally forms sII hydrate, we checked whether the structural change of CH_4 hydrate crystal occurs during the hydrate formation. The behavior of MSZW of CH_4 hydrate was investigated with CP hydrate seeds and compared the effectiveness with sodium dodecyl sulfate (SDS). Lastly, we determined the correlation coefficients based on the hydrate nucleation theory for estimating the MSZW of CH_4 hydrate in the presence of SDS and CP hydrate seeds. This work can shed light on the hydrate nucleation process with kinetic hydrate promoters and provide a way to predict the kinetics of seed-induced hydrate nucleation with the cumulative nucleation potential.

EXPERIMENTAL SECTION

1. Materials

Methane (CH_4, with a purity of 99.95%) was supplied by Special Gas (Republic of Korea). Deionized water was made by a Millipore Direct-Q purification system with a resistivity of 18.2 MΩ cm^{-1}. Cyclopentane (CP, with a purity of 98%), tetrahydrofuran (THF, with a purity of 99.9%), and sodium dodecyl sulfate (SDS, with a purity of ≥99%) were purchased from Sigma-Aldrich. Ethanol (CH_3CH_2OH, with a purity of 99.5%) was purchased from Daejung Chemicals & Metals Co. Ltd. (Republic of Korea).

2. Crystal Structure Analysis of the CH_4 Hydrate Using Synchrotron HRPD

Mixed hydrate samples were prepared with different concentrations of 0, 0.556, and 1.112 mol% of CP or THF below the stoichiometric concentration (5.56 mol%) for sII hydrate formation. 25 mL of CP or THF solution was loaded into a high pressure reactor and then the reactor was flushed with methane gas to remove residual air. The reactor was sealed and immersed into an ethanol circulation bath, and the initial pressure and temperature were set to be 7 MPa and 285.15 K. After stabilization of temperature and pressure, the reactor was cooled to 274.15 K with a cooling rate of 4 K/hr and held for 3 hrs. Next, the temperature was increased to 285.15 K with a heating rate of 4 K/hr, and held for 3 hrs. This temperature sequence was repeated three times to minimize the portion of hexagonal ice in the reactor. The reactor was then quenched in liquid nitrogen and methane was vented to the fume hood immediately. The recovered hydrate samples were finely ground with a 200 μm sieve for a precise spectroscopic analysis. The HRPD patterns were recorded at the HRPD beamline (9B) facility of the Pohang Accelerator Laboratory (PAL) in the Republic of Korea. During the measurements, the $\theta/2\theta$ scan mode with a fixed time of 1 s, a step size of 0.01° for 2θ=5-125.5°, and the beamline with a wavelength of 1.5167 Å was used for each sample. The hydrate sample stored in liquid nitrogen was quickly transferred to the precooled sample stage, and the experiment was conducted at 77 K to minimize possible sample damage. The obtained patterns were analyzed by the Le Bail fitting method using profile matching of the Fullprof Program to determine the crystal structures [24].

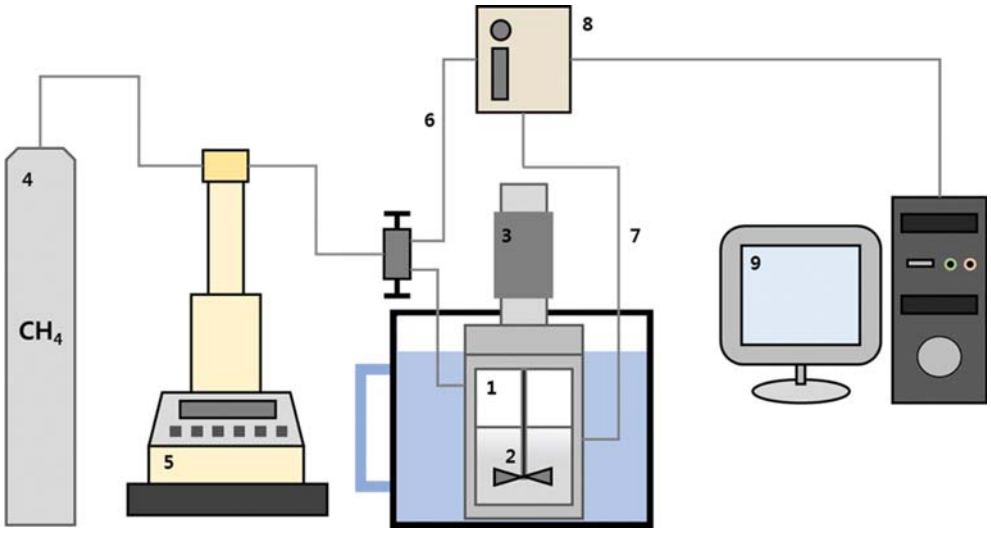

Fig. 1. Schematic diagram of the measurement setup for the MSZW experiment.

1. High pressure hydrate reactor
2. Stirring impeller
3. Magnetic motor
4. CH_4 gas bomb
5. Syringe pump
6. Pressure transducer
7. Thermocouple
8. Data collecting unit
9. Data processing computer

3. MSZW Measurements of the CH_4 Hydrate

To compare the effect of several hydrate promoters on the MSZW of CH_4 hydrate, we prepared 25 mL of sample solutions with various additives: deionized water, 500 ppm SDS solution, 1.0 wt% CP hydrate seed-dispersed solution, and 1.0 wt% CP hydrate seed+500 ppm SDS solution. Here, we stress that the CP hydrate seed-dispersed solution contains 1.0 wt% of CP hydrate crystals in 25 mL of pure water, not 1.0 wt% of liquid CP in the solution. The CP hydrate seed solution was produced by freeze-thaw of the liquid CP solution [25,26]. The liquid CP solution was periodically shaken to disperse CP hydrate crystals when the solution was frozen at 243.15 K and then melted at 277.15 K. In addition, 0.2-1.8 wt% CP hydrate seed solutions were prepared in the same manner to investigate the effect of the amount of hydrate seeds on the MSZW of CH_4 hydrate.

Fig. 1 presents a schematic diagram of the experimental set-up for measuring the MSZW of CH_4 hydrate. A high pressure cell with a stirring impeller connected by a magnetic motor was adopted and the solution was mixed with a stirring speed of 300 rpm during hydrate crystallization. The pressure and temperature (*P-T*) of the reactor were simultaneously recorded at an acquisition interval of 30 s using a four-wire Pt-100 Ω probe (±0.05% accuracy) and a pressure transducer (PMP5073, Druck, ±0.02% accuracy). The measured *P-T* data were collected on a data acquisition computer through an I/O expansion unit (i-87K5, ICP DAS co. Ltd.).

After 25 mL of the sample solution was loaded into the cell, the cell was immersed into an ethanol circulation bath. The temperature of the cooling bath was maintained at 288.15 K, and the methane gas was pressurized up to 8 MPa using a syringe pump. In this condition, the system did not reach a metastable condition of CH_4 hydrate, but a metastable condition of CH_4-CP binary hydrate; the pressure of our system was between the equilibrium pressure of CH_4 hydrate (10.65 MPa [27]) and that of binary CH_4-CP hydrates (1.093 MPa [28]) at 288.15 K, respectively. Thus, CH_4 molecules were able to be encaged with vacant small cavities of the CP hydrate seeds during CH_4 pressurization. After the stabilization, the temperature was cooled to 285.15 K at a cooling rate of 1 K/hr, and then the cooling rate was decreased to 0.2 K/hr. The temperature was slowly lowered until a sudden pressure drop occurred, and the *P-T* data were simultaneously collected to find the detectable point of the MSZW of CH_4 hydrate.

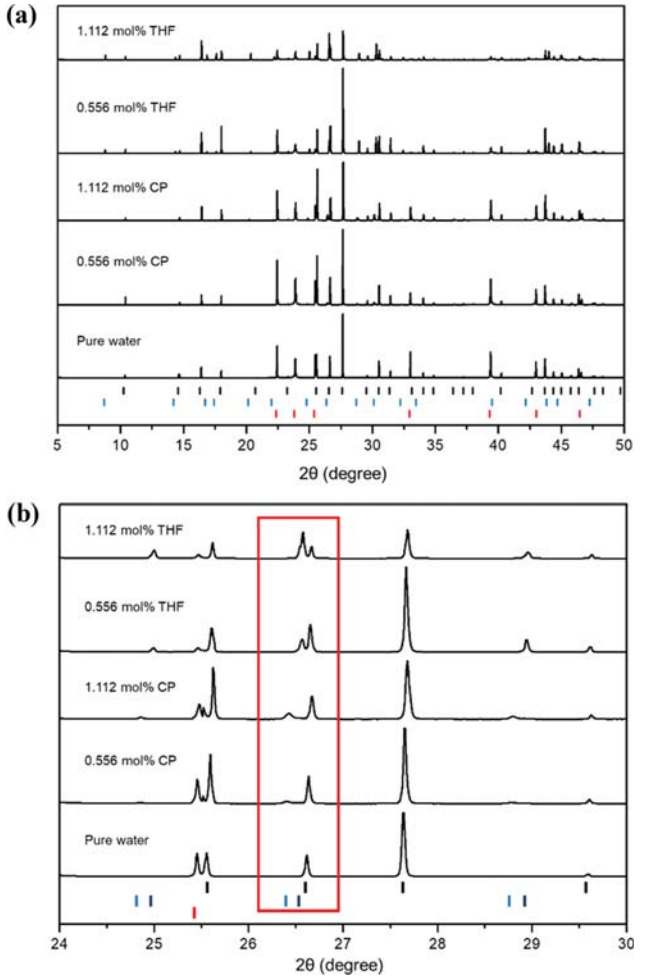

Fig. 2. High resolution power diffraction patterns of pure CH_4 hydrate, CH_4+CP, and THF+CH_4 mixed hydrates prepared with 0, 0.556, 1.112 mol% CP and THF. (a) Overall diffraction patterns in 2θ=5-50°. Black tick marks, cubic *Pm$\bar{3}$n* phases; blue tick marks, cubic *Fd$\bar{3}$m* phases; red tick marks, hexagonal *P6/mmc* phases. (b) Enlarged patterns in 24-30° of HRPD patterns. (5 1 1) plane of the sII hydrate phase and (3 2 0) plane of the sI hydrate phase are specified in the red rectangle. Tick marks of sII hydrate phase are distinguished by blue tick marks for CP+CH_4 sII hydrate and dark blue for THF+CH_4 sII hydrate.

RESULTS AND DISCUSSION

1. Crystal Structure of the CP+CH_4 and THF+CH_4 Hydrates

Fig. 2 shows the HRPD patterns of CH_4 hydrate samples prepared with various concentrations of CP and THF. The structures of the hydrate samples were identified from a comparison of distinct patterns of three well-known hydrate structures (sI, sII, and sH). The sII hydrate phase can be detected even with a small amount of 0.556 mol% CP and THF, which is 10% of the stoichiometric concentration of sII hydrate (5.56 mol%), as shown in Fig. 2(a). Interestingly, we could observe slightly different HRPD patterns between CP+CH_4 and THF+CH_4 mixed hydrates. Whereas, the peak intensities of sII hydrate phase in the CP+CH_4 mixed hydrate gradually increased as the concentration of CP rose, those of sII hydrate phase in the THF+CH_4 mixed hydrate sharply increased. In the case of CP+CH_4 mixed hydrate, the trend was similar to that in our previous work, presenting a CH_4+CP mixed hydrate with 0.0556, 0.556, and 2.78 mol% CP analyzed by powder X-ray diffraction [23]. The intensity of representative peaks of sII hydrate phases was almost equivalent to the that of sI hydrate phase with 2.78 mol% CP, half of the stoichiometric amount of sII hydrate. Thus, it appears that THF strongly induced sII hydrate formation during the CH_4 enclathration, while CP retained the intrinsic structure of CH_4 hydrate structure (cubic *Pm$\bar{3}$n*) even with the addition of CP during hydrate crystallization.

For some binary hydrates it is known that small guest molecules (e.g. CH_4 and H_2) are captured in the small cavities as well as

large cavities of sII or sH hydrate. This phenomenon is known as the tuning effect, which can be induced by the specific concentration region of large guests below their stoichiometric amount during hydrate formation [29-31]. THF is one of the well-known guest molecules that leads to gas guest tuning to improve the storage efficiency of gas molecules in the hydrate medium [29,31], and thus the peak intensity of sII hydrate phase can be highly increased by CH_4 enclathration into the large cavity of tuned sII hydrate. Contrary to the THF+CH_4 mixed hydrate, the peak from the sII hydrate phase shows that CP does not enable CH_4 molecules to construct their own sII hydrate crystals and the sII hydrate phase was gradually increased over the concentration of CP. Although THF and CP have similar chemical structures, their miscibility in water is different due to the substituted oxygen atom in the pentagonal ring of THF. In addition, it is known that the tuning effect is induced by the strong thermodynamic promotion effect and high interaction between guest and water molecules in the hydrate crystallization process [30]. However, CP must be excluded during the hydrate formation owing to its low immiscibility in water. Thus, we expected that the low concentration of CP would not be able to strongly induce CH_4 enclathration into the large cavities of sII hydrate, and remaining water would be fully converted to sI CH_4 hydrate. At this point, it is considered that the inclusion of CH_4 molecules contributed to the sI hydrate formation even with the injection of CP hydrate seeds in the MSZW experiments, where the corresponding parameters were estimated from the kinetic model based on the hydrate nucleation theory.

2. Metastable Zone Width of CH_4 Hydrate Formation

To quantify the effect of CP hydrate seeds on the methane hydrate nucleation, we estimated the effective surface energy with different amounts of additives and the concentration of nucleation site varied with the amount of CP hydrate seeds. These parameters can be obtained from the theoretical nucleation rate of methane hydrate based on the hydrate nucleation theory. In section 2, the distributions of MSZW are analyzed with various types of additives and concentrations of CP hydrate seeds, and how these results can be related with the effective surface energy (σ_{ef}) which defines the critical work to generate a permanent hydrate nucleus is discussed. In section 3, the process for the calculation of the theoretical induction time and the nucleation potential of the methane hydrate crystallization with the term of chemical potential is described. Section 4 explains how to estimate the effective surface energy, the concentration of nucleation sites and the correlation between the concentration of CP hydrate seeds and the nucleation sites.

Since the generation of a critical nucleus cannot be directly observed, we defined the nucleation point when the CH_4 pressure of the *P-T* profile starts to be lower than that of the CH_4 pressure curve with no hydrate formed [15]. Fig. 3 presents how we measured the MSZW of CH_4 hydrate from the *P-T* diagram. The system has a positive potential of hydrate nucleation in a supersaturation condition when the pressure and temperature of the system are located in the region where the CH_4 pressure curve lies above the CH_4 hydrate equilibrium curve. At the initial stage of cooling, the measured *P-T* profile closely overlaps the CH_4 saturation curve, and this means the hydrate nucleus cannot reach the critical size

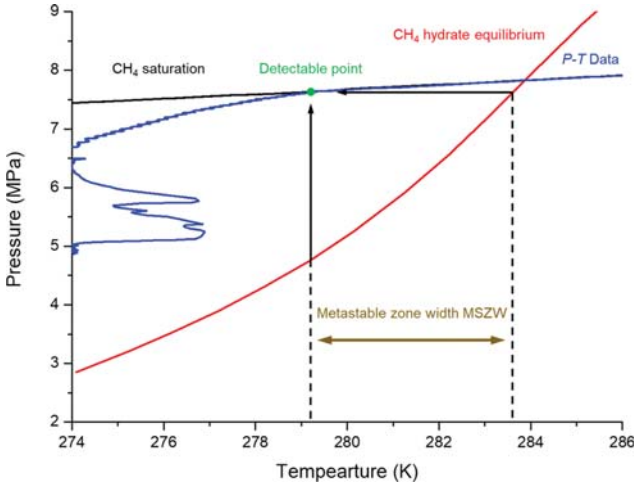

Fig. 3. Pressure and temperature profiles during CH_4 hydrate formation (blue solid line). The black solid line is for the CH_4 pressure curve with no hydrate formed [15] and the red line is for the CH_4 hydrate equilibrium curve. The MSZW of CH_4 hydrate was determined by the gap between the temperature at the detectable point and the equilibrium temperature of CH_4 hydrate corresponding to the pressure at the detectable point.

to grow continuously. In classical nucleation theory, the critical nucleation work (W^*) and critical number of hydrate crystallite units (n^*) depend on the supersaturation as follows [14]:

$$W^* = \frac{4c^3 v_h^2 \sigma_{ef}^3}{27\Delta\mu^2} \quad (1)$$

$$n^* = \frac{8c^3 v_h^2 \sigma_{ef}^3}{27\Delta\mu^3} \quad (2)$$

where c is a shape factor, v_h is the volume of a hydrate crystallite unit, σ_{ef} is an effective surface energy, and $\Delta\mu$ is supersaturation, the difference in the chemical potential between hydrate crystallite units in the solution and solid hydrate phases. Hence, the critical nucleus demands larger amounts of hydrate crystallite units at a lower supersaturation condition. A sudden pressure drop was observed at the detectable point where the pressure deviation between the *P-T* data curve and the CH_4 hydrate equilibrium curve occurred. We defined the MSZW of CH_4 hydrate as the gap of temperature between the detectable point and the corresponding point on the CH_4 equilibrium curve, as shown in Fig. 3. Therefore, it represents the cumulative nucleation potential of CH_4 hydrate; the relationship between the nucleation potential and the MSZW of CH_4 hydrate will be discussed later.

Fig. 4 shows the MSZW of CH_4 hydrate with respect to the presence of kinetic hydrate promoter (SDS) and the concentration of CP hydrate seeds. The average MSZW was 3.39±0.55 K without any additives, but it decreased with the addition of SDS: 2.31±0.39 with 500 ppm SDS, 1.32±0.24 with 1 wt% CP hydrate seeds, and 1.00±0.11 with the combined SDS and CP hydrate seeds, as shown in Fig. 4(a). CP hydrate seeds more strongly affected the MSZW of CH_4 hydrate than that of SDS, and they had a synergistic pro-

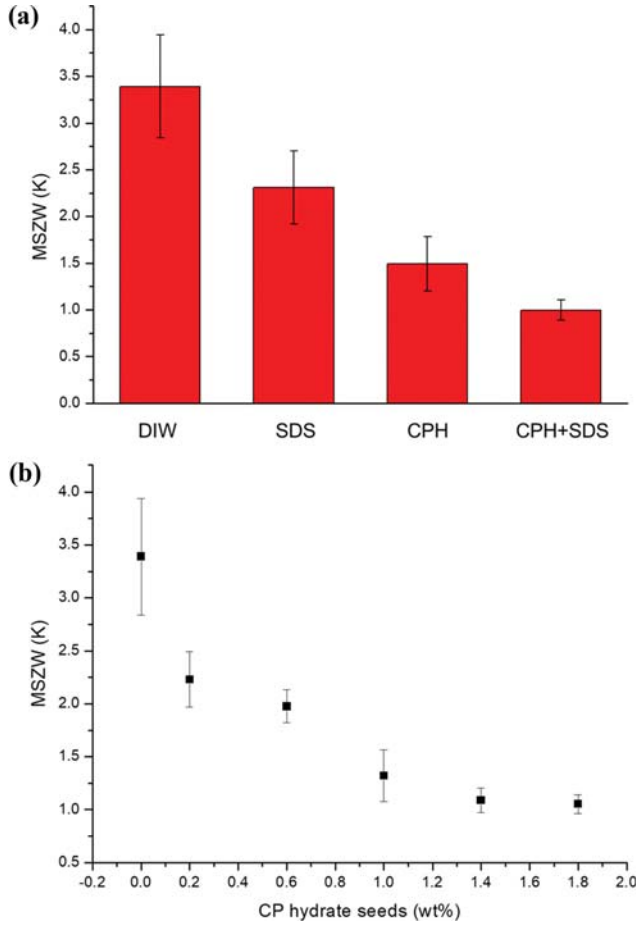

Fig. 4. (a) MSZW of CH_4 hydrate with the various types of hydrate promoters: none, 500 ppm SDS, 1 wt% CP hydrate seeds, and the combination of 1 wt% CP hydrate seeds +500 ppm SDS. (b) MSZW of CH_4 hydrate with various concentrations of CP hydrate seeds.

motion effect on the hydrate nucleation process. The heterogeneous nucleation is more energetically favorable than homogeneous nucleation, and it depends on the contact angle θ between the surface of the crystal and the substrate. It is directly related to the effective surface energy (σ_{ef}), one of parameters in the critical nucleation work (W^*). At the hydrate-water-substrate interface, the effective surface energy can be calculated as follows [32]:

$$\Psi=\left[\frac{1}{4}(2+\cos\theta)(1-\cos\theta)^2\right]^{1/3} \quad (3)$$

$$\sigma_{ef}=\Psi\sigma \quad (4)$$

where Ψ is the numerical factor for cap-shaped clusters on the substrate and σ is the specific surface energy of the hydrate and water interface. The effective surface energy σ_{ef} is equivalent to the specific surface energy in the homogeneous nucleation, and this means the hydrate nucleation prefers the partially-wetted surface of the substrate over the inside of the bulk water phase.

In our system, the stainless steel hydrate reactor wall can serve as a site for heterogeneous nucleation [21], and thus SDS can reduce the MSZW of CH_4 hydrate due to its capability as a surfactant in reducing the interfacial energy between the hydrate crystal and the stainless steel wall. At this point, the CP hydrate seed is also a solid substrate, and the surface of the hydrate seed can become a new nucleation site for CH_4 hydrate. Thus, the MSZW of CH_4 hydrate with CP hydrate seeds is much lower than that without any hydrate promoters despite the fact that the concentration of CP does not have an effect on the equilibrium of CP+CH_4 hydrate, and the effective surface energy for the heterogeneous nucleation on the CP hydrate seeds can be decreased with the addition of SDS. Thus, the CP hydrate seeds provide energetically favorable nucleation sites for CH_4 hydrate nucleation, and this effect is much higher than that of the stainless steel wall.

Since the surface of CP hydrate seeds is the nucleation site for the heterogeneous nucleation, the nucleation rate is directly affected by the amount of CP hydrate seeds in the system. The MSZW of CH_4 hydrate is monotonically decreased as the concentration of CP hydrate seeds increases, as shown in Fig. 4(b). This result indicates that the CP hydrate seed provides a site for heterogeneous nucleation, thereby inducing rapid hydrate nucleation and diminishing the MSZW of CH_4 hydrate. Interestingly, the slope of the MSZW curve is decreased as the concentration of CP hydrate seeds increases, with the curve reaching a plateau at 1.8 wt% of CP hydrate seeds. Thus, the expanded nucleation site was not linearly proportional to the promotion effect on the hydrate nucleation, and this effect was saturated at a high concentration of CP hydrate seeds.

3. Calculation of the Nucleation Potential Based on the Hydrate Nucleation Theory

To analyze the correlation between the kinetics of hydrate nucleation and the amount of CP hydrate seeds, kinetic parameters were estimated with the experimental MSZW data based on the hydrate nucleation theory. Kashchiev and Firoozabadi derived a series of general expressions for the gas hydrate nucleation process from the definition of supersaturation on the hydrate nucleation to calculate the theoretical induction time in various nucleation systems [14-16]. The supersaturation ($\Delta\mu$) is known as the driving force for the entire crystallization process; the activity coefficient of dissolved gas is determined by the concentration of gas molecules in the aqueous solution. In an isothermal process, $\Delta\mu$ depends on the difference of gas pressure P between the current and equilibrium states. In our system, the pressure and temperature were simultaneously lowered by cooling the hydrate reactor. However, we assumed that the system maintained the temperature within a time interval, because the temperature was lowered by stepwise changes at a cooling rate of 0.2 K/hr. Thus, all kinetic parameters were estimated by the theoretical derivations in the quasi-isothermal regime.

Before the supersaturation ($\Delta\mu$) was calculated from the measured P-T data, the vapor pressure of water was subtracted from the total pressure (P_{tot}) to obtain the partial pressure of CH_4 in each time interval. The Antoine equation was employed to calculate the vapor pressure of water and partial pressure of CH_4 as follows [33]:

$$P_{water}=10^{-3}\exp\left(16.3872-\frac{3885.70}{T-42.98}\right) \quad (5)$$

$$P_{CH_4} = P_{tot} - P_{water} \quad (6)$$

where T is the temperature in the hydrate reactor, and P_{CH_4}, P_{water}, and P_{tot} are the partial pressure of CH_4, water vapor pressure, and total pressure at each measured point, respectively. Also, the equilibrium pressure of CH_4 hydrate (P_{eq}) at a specific temperature was obtained by the interpolation of 20 equilibrium points obtained by experimental data [27] from 273.65 K to 288.15 K. From P_{CH_4} and P_{eq}, the supersaturation ($\Delta\mu$) in the isothermal regime can be calculated by the following equation [16]:

$$\Delta\mu = k_b T \ln\left(\frac{f_{CH_4}}{f_{eq}}\right) + (P_{CH_4} - P_{eq})(n_w v_w - v_h) \quad (7)$$

where k_b is the Boltzmann constant, f_{CH_4} and f_{eq} are the fugacity of CH_4 in actual and equilibrium states, respectively, n_w is the hydration number of sI hydrate, and v_w and v_h are the volumes of water molecules and of a hydrate crystallite unit, respectively.

In an isothermal process, if hydrate crystallites are continuously generated during hydrate nucleation, the stationary nucleation rate (J) and the kinetic constant (A) are described as follows [14]:

$$J = A e^{\Delta\mu/k_b T} \exp\left(-\frac{W^*}{k_b T}\right) \quad (8)$$

$$A = z\varepsilon(4\pi c)^{1/2} v_h^{1/3} D C_e n^{*1/3} C_0 \quad (9)$$

where z is the Zeldovich factor [32], ε is the sticking coefficient of a hydrate crystallite unit to the surface of the hydrate nucleus [34], D is the diffusion coefficient of CH_4 in the solution [35], C_e is the concentration of dissolved CH_4 in the equilibrium state [36], and C_0 is the concentration of nucleation sites in the system. All kinetic parameters were obtained from the corresponding references described in Table 1 except for the concentration of nucleation sites (C_0) because C_0 depends on the contact area between the solution and stainless steel wall or the amount of CP hydrate seeds in the system.

Since instantaneous nucleation cannot be measured by macroscopic observation, the induction time is defined by the time needed to observe the detectable point in Fig. 3. Thus, the volume fraction of a detectable crystal (α) can be calculated from the amount of consumed CH_4 molecules within the first time interval at the detectable point. The fraction (α) was distributed in 10^{-5} order of magnitude, and we used an average value $\alpha = 2.188\times10^{-5}$ ($\pm 1.35\times10^{-5}$) for the calculation of induction time. In addition, the growth rate at initial hydrate formation should be considered to calculate the induction time because the hydrate crystal grew to reach a detectable volume in the experiments. The $\Delta\mu$-independent growth constant (Q) can be described by the following equation [15]:

$$Q = \varepsilon v_h D C_e \delta^{-1} \quad (10)$$

where δ is the thickness of a diffusion stagnant film that is a function of D and the gas-liquid mass transfer coefficient of CH_4 in water (k_L) [37]. The induction time t_i at each point on the *P-T* data can then be obtained from the overall derivation based on the hydrate nucleation theory as follows [15]:

$$S = \exp\left(\frac{\Delta\mu}{k_b T}\right) \quad (11)$$

$$K = \left[\frac{\alpha(1+3m)}{bQ^{3m}A}\right]^{\frac{1}{1+3m}} \quad (12)$$

$$t_i = K[S(S-1)^{3m}]^{-\frac{1}{1+3m}} \exp\left(\frac{4c^3 v_{hl}^2 \sigma_{ef}^3}{27(k_b T)^3 (1+3m)(\log S)^2}\right) \quad (13)$$

where S is the term of the supersaturation, K is the practically $\Delta\mu$-independent factor, b is the shape factor, and m is the numerical factor for the tendency of crystal growth with $b=4\pi/3$ [15] and m=1 [15] for the heterogeneous nucleation process.

If the supersaturation ($\Delta\mu$) is treated as a function of temperature, the induction time is only dependent on the temperature in Eq. (13), but the numerator of $4c^3 v_{hl}^2 \sigma_{ef}^3$ is a unique *T*-independent term in the overall expression of hydrate nucleation. It is referred to as the critical nucleation potential (N), and N is a constant for representing the work to form a critical hydrate nucleus at constant pressure and temperature [17,18]. In the polythermal regime, variation of supersaturation should be considered to calculate the critical nucleation potential (N), and thus the instantaneous nucleation potential (N_{ins}) can be described as follows [17,18]:

$$N_{ins,n} = \frac{\Delta t}{t_{i,n}} N = \frac{N\Delta t}{K_n[S_n(S_n-1)^{3m}]^{-\frac{1}{1+3m}} \exp\left(\frac{N}{27(k_b T_n)^3 (1+3m)(\log S_n)^2}\right)} \quad (14)$$

where Δt is the scale of time interval and the subscript n refers the *n*th time interval measured during the hydrate nucleation. Thus, the MSZW of CH_4 hydrate can be estimated from the equivalent point between the cumulative nucleation potential ($\Sigma N_{ins,n}$) and the critical nucleation potential (N).

Table 1. Crystallization and mass transfer parameters for the calculation of kinetic constant (A) in Eq. (9)

Parameter	Corresponding value or equation	Ref.
z	$\sqrt{W^*/(3\pi k_b T n^{*2})}$	[41]
ε	0.7	[43]
D	$(-2611.7\times1000/T+10648)\times10^{-12}$	[44]
C_e	$f_{eq}N_A/HM_{w,H_2O}$ where, H=83.792T-20711 (Henry's constant)	[45]

4. Estimation of the MSZW of CH_4 Hydrate

The probability of hydrate nucleation is the ratio of the cumulative nucleation potential (ΣN_{ins}) to critical nucleation potential (N), and Fig. 5(a) and (b) show the cumulative nucleation probability for various hydrate promoters and the amount of CP hydrate seeds, respectively. The probability distributions suddenly increase in the vicinity of the MSZW and reach the MSZW within 0.5 K. Interestingly, the slope of each distribution monotonically decreased when the hydrate nucleation proceeded slowly. In the case of 1.4 wt% and 1.8 wt% CP hydrate seeds in Fig. 5(b), the cumulative nucleation potentials promptly reached the critical nucleation potential, and the MSZW of CH_4 hydrate was around 1 K for detecting

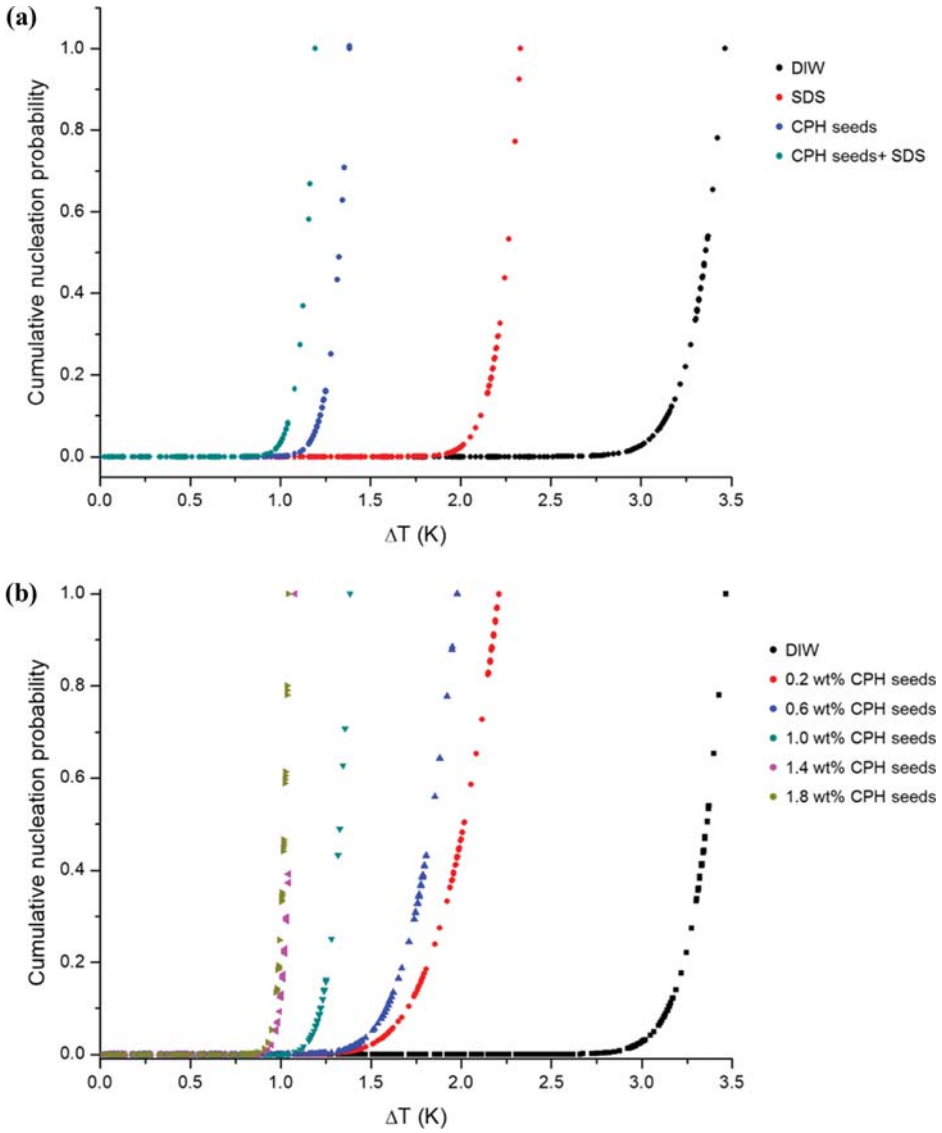

Fig. 5. Cumulative nucleation probability of the MSZWs of CH_4 hydrate varying with the types of hydrate promoters (a) and the concentration of CP hydrate seeds (b).

the hydrate nucleation. The instantaneous nucleation potential is determined by the critical nucleation potential (B), the kinetic constant (A), and the degree of supersaturation (S_n) in Eq. (14). Since the cooling rate is the same for all MSZW experiments, the key factor of hydrate promotion is how to decrease the critical nucleation potential and increase the kinetic constant with the addition of a hydrate promoter.

As mentioned above, the critical nucleation potential represents the environment of the hydrate crystallization system, and thus it is expected that the types of hydrate promoters can significantly affect the change of critical nucleation potential. In particular, the effective surface energy varies with the substrate in the heterogeneous nucleation, and thus the contact angle was estimated by iterations of the cumulative nucleation probability in terms of the type of hydrate promoters. To obtain the contact angle on the stainless steel, the concentration of nucleation site $C_{0,ss}$ is fixed in Eq. (9) as follows [14,15]:

$$C_{0,ss} = A_s/V_s a_w = 1.29\times10^{21}\ m^{-3} \quad (15)$$

where V_s is the volume of solution, A_s is the contact area between the solution and stainless steel wall, and a_w is the area covered by a water molecule on the substrate with $V_s=2.5\times10^{-5}\ m^3$, $A_s=3.76\times10^{-4}\ m^2$, and $a_w=1.1674\times10^{-19}\ m^2$.

The estimated contact angles are 44.17° and 35.26° for the CH_4 hydrate nucleus on the stainless steel wall in the absence and presence of 500 ppm SDS, respectively. However, the concentration of nucleation site for the CP hydrate seed $C_{0,CPH}$ varies with the amount of CP hydrate seeds in the reactor. At this point, we assumed that $C_{0,CPH}$ reached the theoretical maximum value of the heterogeneous nucleation [14], $3.34\times10^{28}\ m^{-3}$, because the MSZW of CH_4 hydrate converged at 1.8 wt% CP hydrate seed. Using the iteration of cumulative nucleation probability, the estimated contact angle is 24.95° for the CH_4 hydrate crystal on the surface of CP hydrate seeds. The concentration of nucleation sites with 0.2-1.4 wt% CP hydrates

Table 2. Esimated kinetic parameters for the hydrate nucleation theory

Sample solution	Seed (wt%)	θ (°)	σ_{ef} (mJ·m^{-2})	N (J^3)	C_0 (m^{-3})
DIW	0	44.17	6.437	5.27×10^{-60}	1.29×10^{21}
SDS 500 ppm	0	35.26	4.883	2.30×10^{-60}	1.29×10^{21}
CP hydrate seeds	0.2	24.95	3.144	6.15×10^{-61}	7.78×10^{8}
CP hydrate seeds	0.6	24.95	3.144	6.15×10^{-61}	2.32×10^{10}
CP hydrate seeds	1.0	24.95	3.144	6.15×10^{-61}	5.91×10^{17}
CP hydrate seeds	1.4	24.95	3.144	6.15×10^{-61}	6.41×10^{26}
CP hydrate seeds	1.8	24.95	3.144	6.15×10^{-61}	3.34×10^{28}
CP hydrate seeds+SDS 500 ppm	1.0	23.02	2.833	4.49×10^{-61}	5.91×10^{17}

and the contact angle with a combination of SDS and CP hydrate seeds can then be obtained by the same routine. The effective surface energy and the critical nucleation potential were also calculated with the corresponding contact angles. All estimated parameters are presented in Table 2.

To estimate the MSZW of CH_4 hydrate from the amount of CP hydrate seeds, the correlation between $C_{0,CPH}$ and the concentration of CP hydrate seeds should be found to calculate the instantaneous nucleation potential (N_{ins}) without experimental data. In the hydrate nucleation theory, the concentration of nucleation sites (C_0) for the heterogeneous nucleation on the microscopic nucleation-active particles can be expressed by the following [14]:

$$C_0 = C_p N_a \tag{16}$$

where N_a is the number of nucleation-active centers on the particles and C_p is the concentration of particles in the solution. Eq. (16) is modified to consider the distribution of CP hydrates in the reactor and to treat N_a as a function of C_{CPH} as follows:

$$C_{0,CPH} = C_{CPH}^{\beta} N_a(C_{CPH}) \tag{17}$$

where β is the regression coefficients of the distribution of CP hydrate crystals. The efficiency of particle collisions depends on the geometric mean size of the colliding particles, and the efficiency has a log-normal correlation over the geometric average [38]. Thus, we assumed that the number of nucleation-active centers on the particles (N_a) varied with the collision efficiency because the nucleation is directly affected by the frequency of crystallite collisions on the nucleation sites [39,40]. Fig. 6 shows the sigmoidal correlation between the logarithm of $C_{0,CPH}$ and C_{CPH}, and the curve was fitted by the non-linear least squares method using the Trust-Region algorithm of MATLAB R2017a as follows [38]:

$$\log C_{0,CPH} = \beta \log C_{CPH} + \gamma_1\left[\frac{1}{2}+\frac{1}{2}\mathrm{erf}\left(\frac{\log(C_{CPH}/N_A)-\gamma_2}{\sqrt{2}\gamma_3}\right)\right] \tag{18}$$

where N_A is the Avogadro constant and γ_1, γ_2, and γ_3 are the regression coefficients for the correlation between the efficiency of particle collisions and the number of nucleation-active centers on the particles.

Table 3 shows the regressed parameters of Eq. (18), and the adjusted R-square is 0.9891. Using $C_{0,CPH}$ calculated by Eq. (18), the

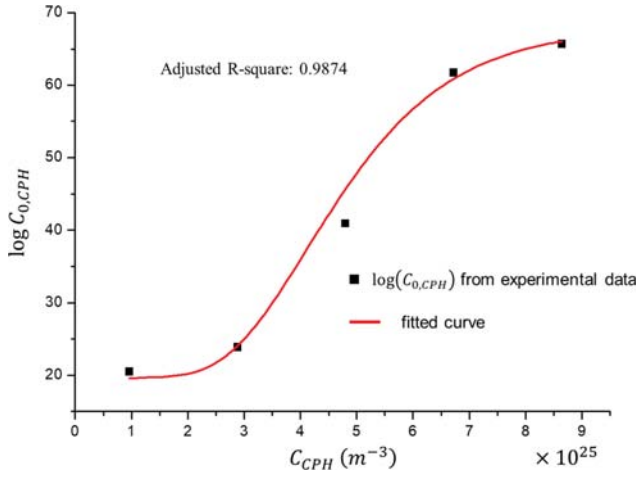

Fig. 6. Correlation between the logarithm of the concentration of nucleation sites for the heterogeneous nucleation with CP hydrate seeds and the concentration of CP hydrate seeds. The curve was fitted by the non-linear least squares method using the Trust-Region algorithm (red solid line).

Table 3. Regression coefficients for the concentration of nucleation sites for CP hydrate seeds

Coefficients	β	γ_1	γ_2	γ_3
Fitted values	0.34	47.55	4.345	0.3495

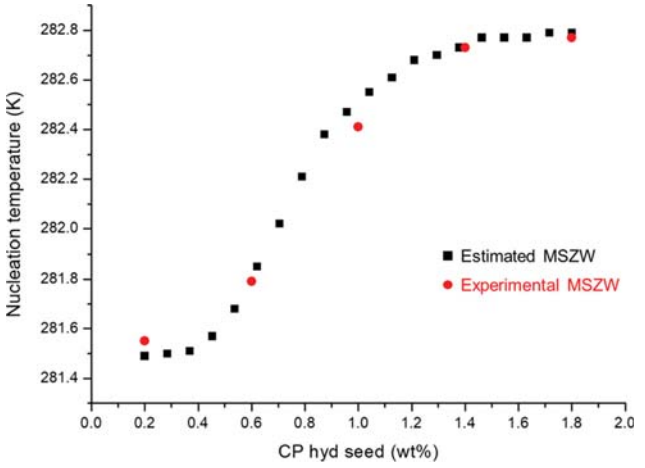

Fig. 7. Experimental and estimated nucleation temperature of CH_4 hydrate over the concentration of CP hydrate seeds.

MSZW of CH_4 hydrate was estimated over the concentration of CP hydrate seeds, as shown in Fig. 7. Even though some deviations between estimated and measured MSZW were observed at lower concentrations, the overall trends of experimental data correlate well with the calculation results.

CONCLUSION

CP hydrate seeds induce CH_4 hydrate nucleation with a low supersaturation in the hydrate-forming system. The HRPD patterns identified that the peak intensity for sII hydrate monotonically decreased as the concentration of CP decreases in the solution, and this indicates the inclusion of CP molecules in the large cavity of sII hydrate cannot significantly induce a tuning effect of CH_4 enclathration in the sII hydrate; the remaining water was converted to sI hydrate with the inclusion of CH_4 molecules after the formation of fully-occupied CH_4+CP binary sII hydrate. The MSZW of CH_4 hydrate diminished with the addition of kinetic hydrate promoters of SDS and CP hydrate seeds. In particular, the CP hydrate seeds greatly promoted hydrate nucleation and showed a synergetic effect with SDS. Furthermore, the MSZW of CH_4 hydrate was inversely proportional to the concentration of the CP hydrate seeds, and the curve of MSZW converged at 1.8 wt%. To analyze the effect of hydrate promoters, the kinetic parameters were estimated from the hydrate nucleation theory, and the effective surface energy and the concentration of nucleation sites varied with the type of hydrate promoters and the amount of CP hydrate seeds, respectively. In addition, the correlation between the concentration of nucleation sites for the CP hydrate seeds ($C_{0,CPH}$) and of the CP hydrate seeds (C_{CPH}) was fitted by non-linear least squares analysis. Using this correlation of $C_{0,CPH}$, the MSZW of CH_4 hydrate was calculated from the cumulative nucleation probability, and the estimated MSZW of CH_4 hydrate was fairly consistent with the experimental results. Thus, the CP hydrate seeds not only induce rapid hydrate formation with a short induction time, but also decrease the MSZW of the crystallization process to generate the hydrate nucleus with low supersaturation.

ACKNOWLEDGEMENTS

The authors are grateful for financial support from the Mid-career Researcher Program through NRF grants (NRF-2017R1A2B4008586) funded by the Ministry of Science, ICT, and Future Planning.

REFERENCES

1. Y.-H. Ahn, S. Moon, D.-Y. Koh, S. Hong, H. Lee, J. W. Lee and Y. Park, *Energy Storage Mater.*, **24**, 655 (2020).
2. M. R. Walsh, C. A. Koh, E. D. Sloan, A. K. Sum and D. T. Wu, *Science*, **326**, 1095 (2009).
3. S. Potdar, J. W. Lee and S. Lee, *Korean J. Chem. Eng.*, **33**, 3216 (2016).
4. M. Cha, K. Shin and H. Lee, *Korean J. Chem. Eng.*, **34**, 2514 (2017).
5. J. Min, Y.-H. Ahn, S. Baek, K. Shin, M. Cha and J. W. Lee, *J. Phys. Chem. C*, **123**, 20705 (2019).
6. S. Baek, J. Min and J. W. Lee, *Rsc Adv.*, **5**, 58813 (2015).
7. M. J. Cha, H. Lee and J. W. Lee, *J. Phys. Chem. C*, **117**, 23515 (2013).
8. J. S. Zhang, C. Lo, P. Somasundaran and J. W. Lee, *J. Colloid Interface Sci.*, **341**, 286 (2010).
9. W. Lee, S. Baek, J. D. Kim and J. W. Lee, *Energy Fuel*, **29**, 4245 (2015).
10. S. Baek, J. Min, Y. H. Ahn, M. Cha and J. W. Lee, *Energy Fuel*, **33**, 523 (2019).
11. A. Ahuja, A. Iqbal, M. Iqbal, J. W. Lee and J. F. Morris, *Energy Fuel*, **32**, 5877 (2018).
12. J. S. Zhang, S. Lee and J. W. Lee, *Ind. Eng. Chem. Res.*, **46**, 6353 (2007).
13. V. Mohebbi, R. M. Behbahani and A. Naderifar, *Korean J. Chem. Eng.*, **34**, 706 (2017).
14. D. Kashchiev and A. Firoozabadi, *J. Cryst. Growth*, **243**, 476 (2002).
15. D. Kashchiev and A. Firoozabadi, *J. Cryst. Growth*, **250**, 499 (2003).
16. D. Kashchiev and A. Firoozabadi, *J. Cryst. Growth*, **241**, 220 (2002).
17. H. Y. Yang and A. J. Florence, *Crystengcomm*, **19**, 3966 (2017).
18. H. Y. Yang, *Crystengcomm*, **17**, 577 (2015).
19. L. D. Shiau, *J. Cryst. Growth*, **450**, 50 (2016).
20. B. Sowa and N. Maeda, *Energy Fuel*, **29**, 5692 (2015).
21. E. F. May, V. W. Lim, P. J. Metaxas, J. W. Du, P. L. Stanwix, D. Rowland, M. L. Johns, G. Haandrikman, D. Crosby and Z. M. Aman, *Langmuir*, **34**, 3186 (2018).
22. J. S. Zhang and J. W. Lee, *Energy Fuel*, **23**, 3045 (2009).
23. S. Baek, Y. H. Ahn, J. S. Zhang, J. Min, H. Lee and J. W. Lee, *Appl. Energy*, **202**, 32 (2017).
24. J. Rodriguezcarvajal, *Physica B*, **192**, 55 (1993).
25. J. S. Zhang, C. Lo, A. Couzis, P. Somasundaran, J. Wu and J. W. Lee, *J. Phys. Chem. C*, **113**, 17418 (2009).
26. J. H. Song, A. Couzis and J. W. Lee, *Langmuir*, **26**, 9187 (2010).
27. E. D. Sloan and C. A. Koh, *Clathrate hydrates of natural gases*, CRC Press (Taylor & Francis Group) (2008).
28. B. Tohidi, A. Danesh, A. C. Todd, R. W. Burgass and K. K. Ostergaard, *Fluid Phase Equilib.*, **138**, 241 (1997).
29. D. Y. Kim, J. Park, J. W. Lee, J. A. Ripmeester and H. Lee, *J. Am. Chem. Soc.*, **128**, 15360 (2006).
30. Z. M. Aman, K. Olcott, K. Pfeiffer, E. D. Sloan, A. K. Sum and C. A. Koh, *Langmuir*, **29**, 2676 (2013).
31. H. Lee, J. W. Lee, D. Y. Kim, J. Park, Y. T. Seo, H. Zeng, I. L. Moudrakovski, C. I. Ratcliffe and J. A. Ripmeester, *Nature*, **434**, 743 (2005).
32. D. Kashchiev, *Nucleation: Basic Theory with Applications*, Butterworth-Heinmann (2000).
33. J. M. Smith, H. C. van Ness and M. M. Abbott, *Introduction to Chemical Engineering Thermodynamics*, McGraw-Hill (2005).
34. J. Skrotzki, P. Connolly, M. Schnaiter, H. Saathoff, O. Mohler, R. Wagner, M. Niemand, V. Ebert and T. Leisner, *Atmos. Chem. and Phys.*, **13**, 4451 (2013).
35. P. A. Witherspoon and D. N. Saraf, *J. Phys. Chem.*, **69**, 3752 (1965).
36. K. Lekvam and P. R. Bishnoi, *Fluid Phase Equilib.*, **131**, 297 (1997).
37. V. Mohebbi, A. Naderifar, R. M. Behbahani and M. Moshfeghian, *Petrol. Sci. Technol.*, **32**, 1418 (2014).
38. M. J. Hounslow, E. J. W. Wynn, M. Kubo and K. Pitt, *Chem. Eng. Sci.*, **101**, 731 (2013).
39. D. Vollhardt, *Adv. Colloid Interface*, **47**, 1 (1993).
40. D. Vollhardt, M. Ziller and U. Retter, *Langmuir*, **9**, 3208 (1993).